

Analysis of Orbital Configurations for Millimetron Space Observatory

A. G. Rudnitskiy^{1,*}, P. V. Mzhelskiy¹, M. A. Shchurov¹, T. A. Syachina¹, P. R. Zapevalin¹

*Astro Space Center, Lebedev Physical Institute, Russian Academy of Sciences,
Profsoyuznaya str. 84/32, Moscow, 117997, Russia*

Abstract

In this contribution a primary feasibility study of different orbital configurations for Millimetron space observatory is presented. Priority factors and limitations were considered by which it is possible to assess the capabilities of a particular orbit. It included technical and scientific capabilities of each orbit regarding the fuel costs, satellite observability, the quality of very long baseline interferometric (VLBI) imaging observations and source visibilities.

Keywords: celestial mechanics, orbit design, methods: numerical, space vehicles, interferometry

2010 MSC: 70F15

1. Introduction

Millimetron observatory is the next generation space mission that is currently under development and planned to be launched after 2029. The active phase of scientific program preparation for Millimetron mission started in 2019. This mission is aimed to study the Universe at different scales, starting with protoplanetary disks in the Galaxy to the study of subtle cosmological effects [1]. To cover all the scientific tasks, Millimetron observatory will have two observing modes: the single-dish mode and the space-ground interferometer (space-ground

*Corresponding author

Email address: arud@asc.rssi.ru (A. G. Rudnitskiy)

VLBI).

10 Scientific tasks for single-dish mostly correspond to the sub-mm and far-
infrared (FIR) wavelength ranges. The tasks are divided into a set of direc-
tions: cosmology (observations of CMB spectral distortions), compact heavily
obscured galaxy nuclei, study of filaments and magnetic fields on various scales,
star and planet formation, gravitational lensing, SZ effect, solar system and
15 search for water trail and complex molecules in the spectra of various cosmic
sources and origin of the life in the Universe. Single-dish mode will include a set
of instruments aimed covering the wavelength range from 0.07 to 3 mm. These
include two camera spectrometers (long and short wave) and high resolution
heterodyne spectrometer (see Section 1.1 for more details). Practically all sci-
20 entific observations in the single dish can be done only in outer space, on board
of a space telescope as the Earth's atmosphere imposes strong restrictions on
the coherent integration time and introduces significant distortions in the signal
especially. Thus, going to space for sub-mm and FIR observations is the only
option. Moreover these science cases apply high requirements to the levels of
25 sensitivity and external sources of noise.

Therefore the antenna and the scientific payload of Millimetron observatory
will be mechanically cooled down to 10 K and 4 K correspondingly. In this
case the orbit around the L2 point of the Sun-Earth system is optimal since the
noise contribution from the Earth and the Moon is blocked by the spacecraft
30 heat shields (see Section 2.1 for more details).

At the same time, the orbit around the L2 point allows to cover about 90%
of the celestial sphere per year. All these factors make it possible to observe
a larger number of sources comparing to near-Earth orbits. In this article, we
would like to dwell in more detail on the VLBI mode of Millimetron mission.

35 Earlier scientific space-VLBI missions such as HALCA and Radioastron have
shown the principal possibility of conducting interferometric observations with
ground-space interferometers [2, 3]. However, before the Millimetron project,
the question of the applicability of this technology to spacecraft in a halo orbit
around the Earth-Sun L2 point has never been raised. This article discusses the

40 very possibility of conducting VLBI observations in such an orbit.

One of the main scientific goals of the space-ground VLBI mode is to observe the shadow and photon rings of black holes. One of the basic techniques in this case is to obtain images of black hole shadows, namely Sgr A* and M87. However, the detection of intrinsic structure of Sgr A* at extremely long base-
45 lines is strongly limited by the scattering due to the observable substructure [4, 5, 6]. Thus, going to the baseline projections larger than $2 - 3 \times 10^4$ km the substructure of the scattering disk of Sgr A* will dominate the intrinsic structure of the source itself at 230 GHz [7]. Another issue is related to the observations of Sgr A* is its high time variability. Characteristic time variabil-
50 ity is about ~ 220 s, which 1000 times less than for M87. Thus, resolving its dynamical structure requires good snap-shot (u, v) coverage [8, 9]. These facts apply additional restrictions to space-VLBI observations of the Galactic center.

High resolution imaging of SMBH with using space-VLBI is currently a very promising area of scientific research (see, for example, [10, 11, 7, 12, 13]), but
55 they all consider only different near-Earth orbits for space telescopes. Imaging the black hole shadow with VLBI straightly depends on the angular resolution, (u, v) coverage and sensitivity of telescopes. Recent experiments of the Event Horizon Telescope allowed to obtain the image of supermassive black hole located in M87 galaxy [14]. Further detailed study of black hole shadows and
60 precise estimation of its parameters requires higher angular resolution [15, 16]. For ground-based VLBI the resolution is straightforward limited by the size of the Earth. Determination of the black hole metric and their parameters, search for the wormhole candidates are also directly related to the spatial resolution of the interferometer. The search task is complicated by the fact that obser-
65 vations must be carried out for a specific sample of sources. In this case the launch of a space radio telescope capable of operating at frequencies compatible with ground observatories is a straightforward way to significantly improve the spatial resolution.

The choice of orbital configuration for the space observatory should be based
70 on the results of analysis of a set of parameters, which include both the technical

aspect of the feasibility of a particular orbital configuration and the scientific potential. Such analysis includes the estimation of fuel costs, spacecraft observability, source visibility, baseline projections (i.e. angular resolution) at which the studied sources can be observed and (u, v) coverage quality.

75 To sum up, one of the main issues of VLBI and, in particular, space-VLBI is the geometry of interferometer that is formed by the telescopes located on the Earth and in space. Obviously, the geometry of space-ground interferometer will depend on the orbital configuration of the space observatory and the total number of participating antennas. For these purposes, we considered and calculated
80 several orbital configurations. The detailed description of these configurations is provided in Section 3.

1.1. Millimetron Observatory

Millimetron space observatory will have 10 meter deployable antenna capable of observing at far-infrared, sub-millimeter and millimeter wavelengths. In
85 order to achieve the best sensitivity for bolometric detectors of the single-dish mode instruments, the antenna will have active and passive cooling systems with cooling down to 10 K and the scientific payload will be located in the container actively cooled down to the temperature of 4 K.

Single-dish mode will have three instruments: long wave camera spectrome-
90 ter (LACS) with 4 sub-bands that cover the frequency range of 100–1000 GHz; short wave camera spectrometer (SACS) with 4 sub-bands that cover the frequency range of 0.7–6.0 THz; heterodyne high resolution spectrometer (MHIFI) with 6 sub-bands that cover the frequency range of 0.5–5.4 THz and one post-cryo sub-band of 500-700 GHz. The sensitivity required for LACS and SACS
95 detectors is $10^{-17} - 10^{-19} \text{ Wt}/\sqrt{Hz}$.

VLBI is going to cover the following frequency bands: 43, 86, 120, 240, 320, 570 GHz. The selection of such frequency ranges for Millimetron observatory is based on the compatibility with ground observatories and proposed scientific cases. The need in VLBI observations at higher frequencies is dictated by the
100 fact that the close surroundings of black holes should be optically thin in order

to be imaged. Additionally, this will minimize the contribution from scattering effects to the resulting images of the Sgr A* black hole shadow in particular [4, 17, 5, 6]. The receivers are expected to be mounted together with a quasi-optical system same as represented in Korean VLBI Network (KVN). Such system will
105 provide the capability to perform simultaneous multi-band VLBI observations [18, 19].

The receivers will support both right and left hand circular polarizations (RCP and LCP correspondingly) with two (upper and lower) sub-bands. The maximum number of digitized channels will be four ($2 \times \text{RCP}$ and $2 \times \text{LCP}$).
110 Bandwidth (IF) of a single channel is 0.97 GHz. The channels could be united in one providing wider total IF bandwidth up to 3.9 GHz (case of one polarization channel and one side band). Currently, the design sensitivity of VLBI frequency ranges is estimated to be 1100, 2700, 5500 and 7200 Jy for 43, 86, 120, 240 and 345 GHz correspondingly. The expected detection limit of 5σ on
115 the baseline Millimetron-ALMA is 5 and 35 mJy for 10 and 1 s of integration time correspondingly for total bandwidth $\Delta\nu = 4$ GHz. The final sensitivity will be known after testing of the on-board receivers performance and antenna efficiency.

Millimetron will have an onboard hydrogen atomic clock with an Allan de-
120 viation of about $\sigma(\tau) = 1.9 \cdot 10^{-15}$ on $\tau \sim 100$ s., which makes it possible to conduct observations in VLBI mode even at frequencies that are much higher (up to 840 GHz) than those to be planned on board [20].

Millimetron will have an onboard memory storage as a buffer storage for the scientific observations. Current volume of this storage is 10 Tb which
125 corresponds to ~ 170 minutes of continuous VLBI observations with $\delta\nu = 1$ GHz bandwidth, 2 sub-bands and 2 polarization channels (RCP & LCP). However, and the storage system is expected to be upgraded up to 100 Tb. This will enable the possibility to observe 10 times longer (~ 1700 minutes) with the same bandwidth and channel configuration.

130 The current implementation of onboard data downlink channel will be capable to transmit the information from the onboard memory storage with a rate

of 1.2 GBit/s. It means that it will take about 18 hours of continuous data transmission to download 10 Tb of the data from the space observatory. This is a critical point that is now being considered for the upgrade and corresponding studies are being performed for it.

More information about the instrumentation, technical parameters and requirements of Millimetron observatory can be found on the official web-site¹.

2. Methods

In this article we have assessed the capabilities of Millimetron space observatory in VLBI mode for several orbital configurations by analyzing such characteristics as (u, v) coverage, the shape and the relative magnitude of synthesized beam, observational capabilities for different orbital configurations. General approach that is used in spacecraft orbital calculations is a numerical integration with various force models. Accuracy of calculated orbits for space missions should be at least 1 cm [21]. There are plenty of different factors that influence the cumulative forces acting on a spacecraft in Earth orbit. For example, along with the central component of the Earth gravitational field there are nonlinear effects that affect the motion of a satellite in its orbit [22]. Also, one should account for the contribution of forces arising from the attraction of other celestial bodies, such as the Moon, the Sun and other.

Orbit integration can be performed by numerical methods, several of them are traditionally used, for example, the Runge-Kutta or the Dormand-Prince methods [23]. Each of them has its own advantages and disadvantages. In this contribution we used the Runge-Kutta method up to 7(8)th order, that was implemented as a part of our ballistic and navigation support software package.

2.1. Spacecraft Constraints

The design features of the Millimetron observatory impose a number of restrictions on possible orbit configurations. The orbit should be selected such as

¹<https://millimetron.ru/en/>

to exclude the shadows from the Earth and the Moon, because of the limited
160 capacity of the onboard power supply systems. In order to avoid direct expo-
sure of the antenna to the Sun there is a limitation in the viewing angles. The
requirements for viewing angles "Sun-Spacecraft-Source" of Millimetron are not
less than 95° . Direct exposure to the Sun can lead to overheat, damage and
failure of high sensitive onboard detectors.

165 The following constraints arise from the requirements for onboard thermal
regulation system – to ensure the required thermal regime of the spacecraft, the
minimal safe height of near-Earth high elliptical orbit (HEO) at perigee must
be not less than 40000 km, antenna must avoid direct exposure from the Sun,
the Earth and the Moon.

170 2.2. Synthesized Beam

Synthesized beam reflects the instantaneous response of interferometer for a
point-source with 1 Jy flux density. It can be represented as a Fourier transform
from the sampling function $S(u, v)$, where the sampling function corresponds
to the (u, v) coverage. With the increasing number of independent antennas N
175 the beam shape will be approaching Gaussian shape.

In general, the beam size and shape can be used to some extent to charac-
terize the quality of VLBI interferometer configuration and the quality of image
reconstruction. This is a simple, but effective way to preliminary evaluate the
VLBI configuration for a given interferometer geometry. The beam shape tells
180 not only about the obtainable angular resolution, but also in some measure
provides the information of (u, v) coverage quality through the evaluation of
the sidelobes effect, which are related to the gaps in the (u, v) coverage leading
to the loss of spatial sensitivity in the configured VLBI array [24]. In case of
space-Earth VLBI the size of the gaps can be substantial [25].

185 2.3. Orbit Integration

Designing the trajectory of a spacecraft during the mission planning can be
highlighted as a separate task. As a rule, the solution of such a problem consists

of two stages: 1) the first approximation, 2) the refinement of obtained approxi-
mation using numerical methods. As such methods, various methods of numeri-
cal integration of differential equations of motion are used. There are methods of
190 single-step and multi-step integration with constant or variable step. The most
widespread of them are the various modifications of the Runge-Kutta method,
that provide the required accuracy with the proper computational speed.

At present, there is a various software that allow, to one extent or another,
195 to solve the problems of designing and predicting the spacecraft trajectories.
Among them there are, for example, GMAT², STK³.

However, in a number of tasks, the use of a third-party software products
lead to a significant complication of the trajectory design process. In this regard,
the use of domestic implementation of the methods of numerical integration is
200 the most practical way. It allows to create more flexible and adaptive software
when solving the problem of the trajectory design.

This work presents the results of the software implementation of the Runge-
Kutta method up to 7(8)th order with a variable adaptive step with the possi-
bility of flexible adjustment of the force model, which includes:

- 205 1. Central gravitational field of the Earth;
2. Non-central effects of the Earth gravitational field (up to the 8th order
inclusively);
3. Gravitational attraction of the solar system bodies: the Sun, the Moon,
Mercury, Venus, Mars, Jupiter, Saturn, Uranus, Neptune and Pluto;

210 2.4. Orbit Design

Since the onboard active cooling system of the Millimetron can provide the
required thermal regimes of antenna and scientific payload for the single-dish
mode only in L2 point orbit, we considered additional near-Earth orbits as the

²GMAT software: <https://software.nasa.gov/software/GSC-17177-1>

³STK software: <https://www.agi.com/products/stk>

second stage of the mission under the assumption of returning the spacecraft
215 from L2 point after completing the scientific program requiring the best sensi-
tivity and deep cooling of the observatory.

Thus, several classes of orbits are considered: elliptical orbits (including
circular) and a halo orbit around the Lagrange point L2. These orbits are the
solution of different problems. In the first case it is a limited two-body problem,
220 in the second it is a limited three-body problem. So the processes are different.

To construct elliptical orbits around the Earth an initial vector, set in Kep-
lerian orbital elements, is translated into J2000 coordinate system. Then, it is
integrated with a variable step, with an initial step of 1 second. Perturbations
are introduced by the force model described above.

225 To construct an orbit around the L2 point of the Sun-Earth system, the
problem of three bodies is considered: the Sun, the Earth, and the spacecraft.
This is a non-linear problem, so numerical integration is used to solve it. To
construct the orbit, an initial approximation is used, in this case, a linear ap-
proximation, then this initial state is integrated forward for the required period.
230 The propagator's capabilities allow for long-term calculations without significant
loss of accuracy on the turn.

The success of any space-VLBI mission directly depends on the accuracy
of orbit determination. High-precision determination of the state vector of the
spacecraft is difficult for the case of a halo orbit around the L2 point of the
235 "Sun-Earth" system, located at a distance of 1.5 million km from the Earth. At
such a distance, it is not possible to use the spacecraft laser positioning method
due to the large signal losses [26]. Therefore, astrometric, radio range and
Doppler measurements are used to determine the position and the velocity of
the spacecraft. They are the input to differential orbit refinement methods such
240 as Least Squares and Kalman Filter [27, 28]. These methods make it possible to
compare the measurement model and real observations and reconstruct the true
orbit. In addition, inaccuracies in determining the position of the spacecraft can
be eliminated by searching for the VLBI fringe at lower frequencies. One way
or another, as a result, it is possible to estimate the spacecraft state vector

245 for a certain epoch, and then, using numerical integration, to predict its further
orbital motion. In turn, for an accurate forecast, it is necessary to have the most
complete force model acting on the space observatory. At the moment, separate
publications are being prepared in our laboratory on the topics of prediction and
reconstruction of the Millimetron orbit including the results of development and
250 testing of the corresponding software packages.

It is planned to carry out trajectory measurements for the Millimetron in
X-band range with a maximum error of 20 m in the slant range and 0.5 mm/s in
the radial velocity, which will be quite enough to determine the residual delays
and successfully obtain correlation for 230 GHz.

255 *2.5. Fuel Consumption*

The flight to L2 point lasts about 100 days. Corrections are made during the
flight to reach the nominal orbit. They are appointed for 10, 20 and 40 days. A
budget of 100 m/s is allocated for these corrections. Further, to maintain the
orbit at the L2 Lagrange point, corrections are carried out approximately every
260 50 days. The total cost of maintaining corrections is about 15 m/s per year.
[29] The offloading of the flywheels was not taken into account.

Two stages for the Millimetron spacecraft mean it is necessary to understand
whether we can change orbits during the lifetime of the project. Two impulses
are required to reach a given high elliptical orbit. The first will lead to deorbiting
265 L2 halo-orbit. The second is performed at the perigee of a given near-earth orbit
to form an ellipse. To do this, firstly, we estimated what impulse it is necessary
to give to the vehicle for deorbiting from L2 halo-orbit into near-earth orbit, as
well as fuel costs.

To find the time interval for deorbiting L2 we sampled several points in
270 the orbit over the course of a year, added a small impulse and integrated the
orbit forward in time, trying to find where the transfer path would intersect
with the given Earth orbit with the same inclination. Then we determined the
impulse for the transition to a given orbit around the Earth using coordinate
descent algorithm. After that we calculated impulse to form an elliptical orbit

275 by velocity difference.

Impulse costs were recalculated into fuel costs using the following parameters: the initial mass of the spacecraft is 10 tons, the specific impulse of the engine is 2842.29 m/s.

2.6. Source Visibility

280 The analysis was based on a list of compact extragalactic sources that were proposed as possible candidates for the observations with Millimetron. Most of these sources were observed and had positive detection in Radioastron space-ground VLBI mission [3, 30, 31]. The list included 386 sources. Coordinates were taken from Radio Fundamental Catalog ⁴, J2000.0 epoch.

285 As ground-based telescopes, we have compiled several sets from all radio telescopes currently available in the world, dividing them into according to the supported frequency bands: 43, 86, 120, 230, 320, 570 GHz. The sets include many telescopes located at around the world, including antennas of largest VLBI networks: EVN, EHT, GMVA, EAVN, VLBA, etc.

290 The visibility of the sources was calculated over 4 years. Sources were considered observable and visible by a telescope if they had an elevation of more than 7° above the horizon. A topocentric coordinate system was introduced using the WGS-84 geodetic system. For Millimetron, the following restrictions were imposed on the visibility of sources: the height of the sources from the
295 ecliptic plane should be in the range of $\{-80^\circ, 80^\circ\}$, while observations were considered possible only in the anti-Solar hemisphere. In addition restrictions were imposed related to the overlapping of the source by the Earth and the Moon. A source was considered unobservable if the difference between the directions to it and to the center of the overlapping body (the Earth or the Moon)
300 was less than 1.1 of the disk radius of this body.

⁴Radio Fundamental Catalog: <http://astrogeo.org/rfc/>

3. Orbital Configurations

The orbits were chosen based on the requirements imposed both by the technical constraints of the spacecraft and by the requirements of the scientific program. First of all, this concerns the requirements for the (u, v) coverage for the imaging sessions in the VLBI mode. Calculated orbits and its parameters are presented Section 4.1.

The considered orbital configurations take into account the experience of previous space missions, generally related to the space-Earth VLBI (HALCA, Astro-G, Radioastron). HALCA and Astro-G used circular near-Earth orbits, providing (u, v) coverage of satisfactory quality for imaging observations [32, 33]. Radioastron mission had a high elliptical near-Earth (HEO) orbit with an apogee of $\approx 330,000$ km, which made it possible to achieve the highest angular resolution of $8 \mu\text{as}$ at the shortest wavelength of the mission ($\lambda = 1.3$ cm) [34, 35].

As for the orbital configurations in the vicinity of the Lagrange point L2 of the Sun-Earth system, Millimetron will be the first mission with VLBI mode to conduct observations there. The following missions can be noted as example of successfully operated and operating space observatories at L2 point: WMAP, Planck, Herschel, GAIA, recently launched Spektr-RG [36] and the upcoming James Webb Space Telescope, WFIRST and others [37, 38, 39, 40, 41, 42].

An important advantage of L2 orbits is the ability to maintain the same position relative to the Sun and the Earth, which makes thermal shielding, cooling and detector calibration much easier. This is especially important for observations in infrared and far-infrared wavelength ranges where it is required to minimize the background noise radiation.

Recent studies demonstrated the capabilities and advantages of the middle near-Earth circular orbits, namely for space-space VLBI with two or more space radio telescopes (see for example, Event Horizon Imager concept [11]). In this work, a set of middle near-Earth circular orbits was considered to check the space-ground VLBI capabilities and the feasibility of these orbital configurations

for Millimetron mission.

4. Results

4.1. Orbits

We have calculated the following set of orbits for Millimetron observatory:
 335 high elliptical near-Earth orbits with the perigee of 40000 km and 100000 km,
 circular near-Earth orbits with the semi-major axis of 40000 km optimized for
 Sgr A* and M87 imaging correspondingly, L2 point orbit. Regarding the circular
 and high elliptical orbit the minimal height of 40000 km is dictated by the
 requirements for thermal regime of the observatory. Flying below this altitude
 340 the observatory won't be able to keep the required temperatures. Parameters
 of calculated near-Earth orbits are shown in Table 1.

Table 1: Parameters of calculated near-Earth orbits for Millimetron space observatory.

Orbit	a , (km)	e	i , ($^{\circ}$)	Ω , ($^{\circ}$)	ω , ($^{\circ}$)
Circular (40000 km)	40000	0	80	70	-70
HEO (Perigee 40000 km)	150000	0.7	100	0	-15
HEO (Perigee 100000 km)	150000	0.3	90	15	0

a – semi-major axis, e – eccentricity, i – inclination, Ω – longitude of the ascending node, ω – argument of periapsis.

The L2 halo orbit period is 1 year, exit from ecliptic plane is 400000 km. This value provides better spacecraft radio visibility from the tracking stations located on the territory of the Russian Federation. Fig. 1 demonstrates projec-
 345 tions of the calculated orbits in geocentric J2000 coordinate system.

The verification of obtained results was carried out with the special software for the ballistic and navigation support of the Spektr-RG flight control center and with the real measurements of the current navigation parameters of the Spektr-RG spacecraft [43]. The results obtained indicate the possibility of pre-
 350 dicting the parameters of spacecraft motion with high accuracy at the stage of

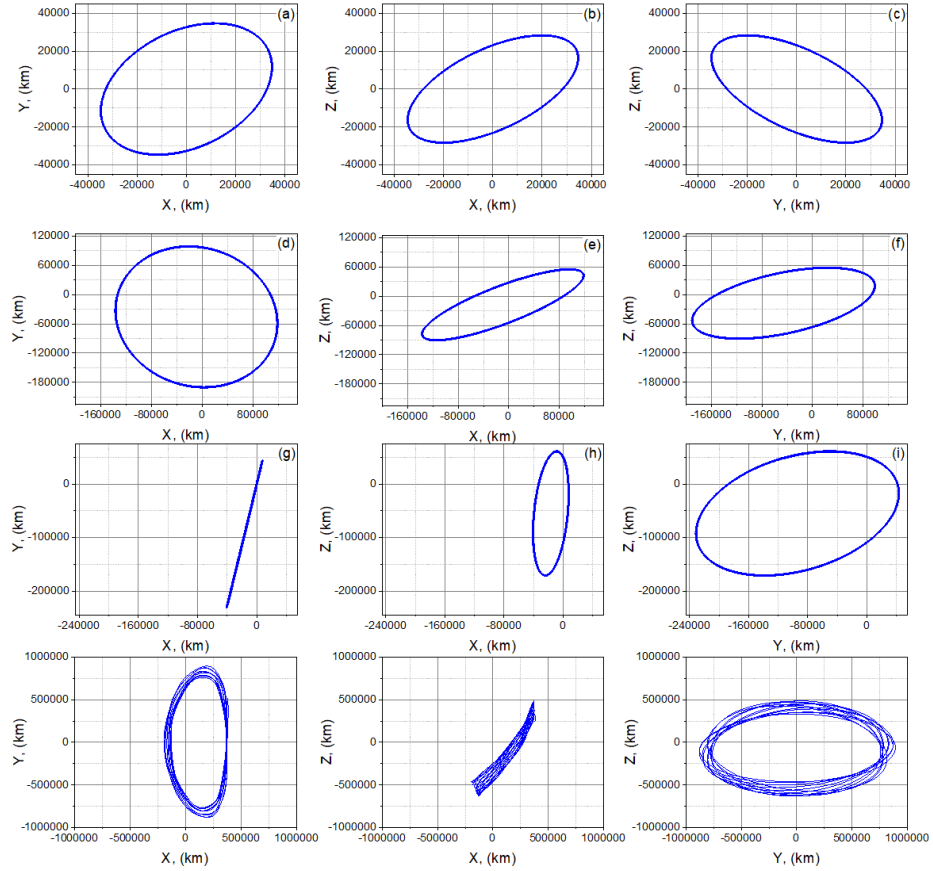


Figure 1: Projections of calculated orbits: circular orbit – XY (a), XZ (b), YZ (c); high elliptical orbit with perigee 40000 km – XY (d), XZ (e), YZ (f); high elliptical orbit with perigee 100000 km – XY (g), XZ (h), YZ (i); orbit around L2 point – XY (j), XZ (k), YZ (l). Coordinate system is geocentric J2000.

flight and in the vicinity of the co-linear libration point L2 of the Sun-Earth system.

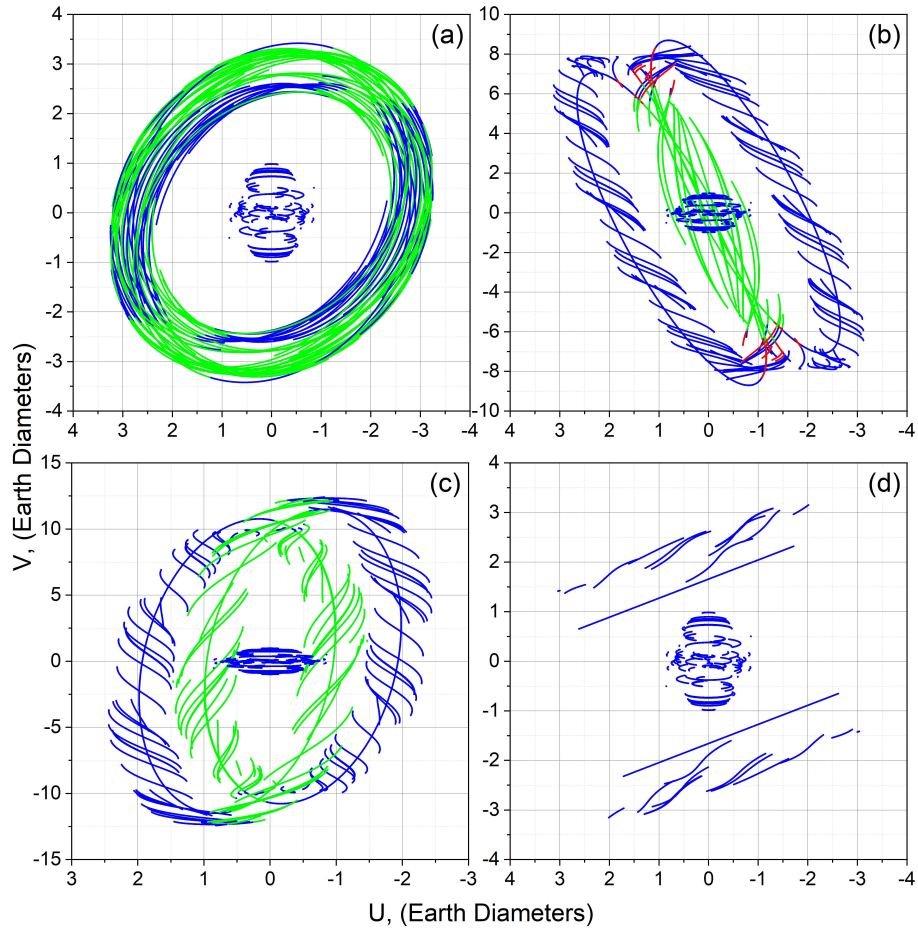


Figure 2: (u, v) coverage for M87 target source: (a) – circular near-Earth orbit, (b) – HEO with 40000 km perigee, (c) – HEO with 100000 km perigee, (d) – L2 point orbit. Blue dots correspond to observations with no constraints, red dots indicate the Moon illumination, green dots indicate the Earth illumination.

This makes it possible to use the developed software at all stages of the design and operation of Millimetron mission, as well as to carry out the necessary
 355 statistical calculations and analysis in order to optimize the planning of scientific observations and to estimate the maximum value of errors in the execution of

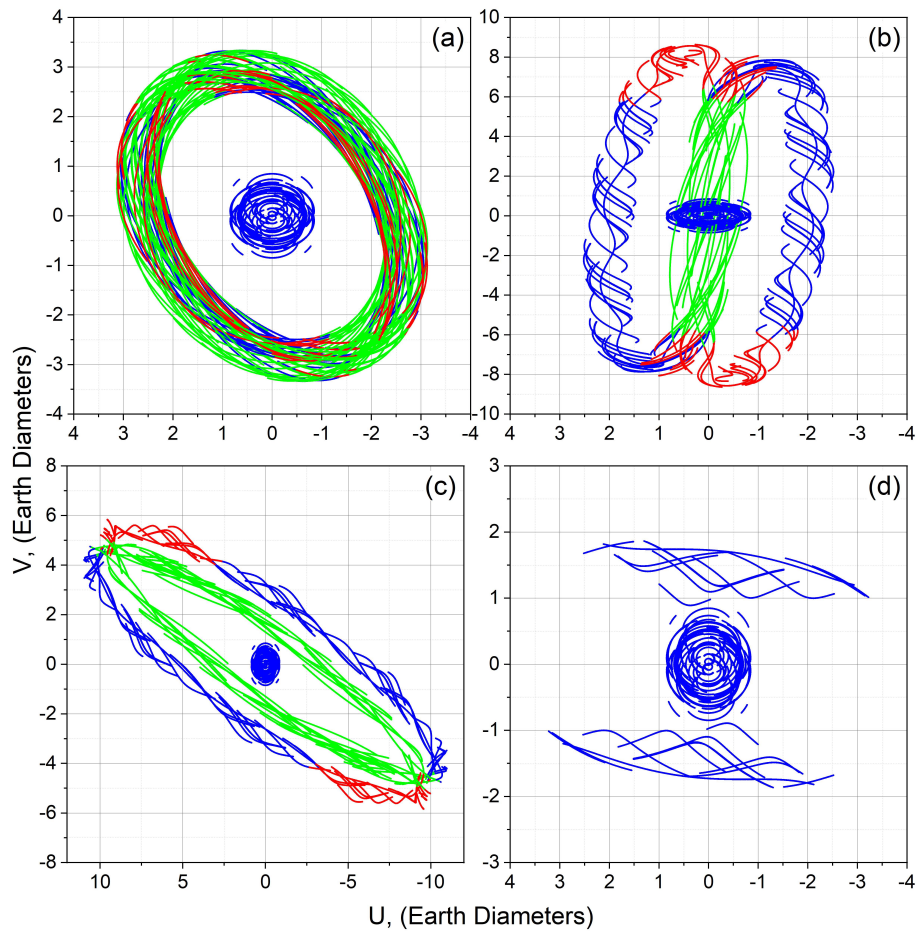


Figure 3: (u, v) coverage for Sgr A* target source: (a) – circular near-Earth orbit, (b) – HEO with 40000 km perigee, (c) – HEO with 100000 km perigee, (d) – L2 point orbit. Blue dots correspond to observations with no constraints, red dots indicate the Moon illumination, green dots indicate the Earth illumination.

dynamic operations.

4.2. Impulse and Fuel Estimates

The results of calculating the cost of the flight are presented in Table 2. Corrections on the flight in L2 are associated with errors in insertion into the launch orbit, so the budget for the flight will be greater than the budget to return . On the return flight, you may not need any correction at all. The time for maintaining the orbit at L2 point was chosen to be 3 years, since this is the time of active cooling of the main mirror of the spacecraft. Deorbiting in L2 is carried out by a short impulse and does not incur large expenditures of fuel. The magnitude of the impulse depends on the specific orbits. In our case, these are impulses of the order of 1 m/s. Near-Earth orbit formation occurs in perigee of the orbit.

Table 2: Impulse and Fuel Estimates.

Maneuver	Impulse, (m/s)	Fuel, (kg)
Correction on flight to the halo-orbit	100	358
Maintaining the halo-orbit (3 years)	45	154
Deorbiting the halo-orbit	0-10	0-33
Correction on flight to the near-earth orbit	0-30	0-100
Near-Earth orbit formation		
Circular (40000 km)	1250	5160
HEO (Perigee 40000 km)	265	914
HEO (Perigee 100000 km)	420	1490

As shown in Table 2 the cost of forming an orbit around the Earth requires a significant amount of fuel. Whereas we have only 800 kg of fuel at our disposal. Therefore, the classical method described in the section 2.5 is not applicable for us. It's worth to pay attention to gravitational maneuvers around the Moon or to change the parameters of high elliptical orbit around the Earth and to consider invariant manifolds. The first one approach requires detailed analysis

Table 3: The list of telescopes used for beam synthesis.

Telescope	Location	Latitude deg, min, sec	Longitude deg, min, sec	SEFD (for 230 GHz) Jy
Millimetron	Space	-	-	~4000
Atacama Large Millimeter Array (ALMA)	Atacama, Chile	23°01'09"S	67°45'12"W	47
Atacama Pathfinder Experiment (APEX)	Atacama, Chile	23°00'21"S	67°45'33"W	4700
Combined Array for Research in Millimeter-wave Astronomy (CARMA)	California, United States	37°16'49"N	118°08'31"W	3500
Greenland Telescope (GLT)	Greenland, Danish Realm	72°35'00"N	38°25'00"W	5000
IRAM 30-m millimeter radio telescope (PV)	Pico Veleta, Spain	37°03'58"N	3°23'34"W	1900
James Clerk Maxwell Telescope (JCMT)	Hawaii, United States	19°49'22"N	155°28'37"W	10500
Kitt Peak National Observatory telescope (KP)	Arizona, United States	31°57'30"N	111°35'48"W	13000
Large Millimeter Telescope (LMT)	Mexico	18°59'09"N	97°18'53"W	4500
Plateau de Bure (PdB)	Alps, France	44°38'02"N	5°54'29"E	1600
Submillimeter Array (SMA)	Hawaii, United States	19°49'27"N	155°28'41"W	6200
Submillimeter Telescope (SMT)	Arizona, United States	32°42'06"N	109°53'28"W	17100
South Pole Telescope (SPT)	Antarctica	90°00'00"S	00°00'00"E	19300

375 due to strict spacecraft orientation constraints while for the second one fuel costs will be smaller if the semi-major axis of HEO is larger or the pericentric distance is smaller.

4.3. Synthesized Beam

Synthesized beams were calculated for each orbit configuration with the
380 ground support of telescopes from Event Horizon Collaboration, considering observing central frequency as 230 GHz and the sensitivities from [44]. The full list of the telescopes that were used in the beam calculation is shown in the Table 3. This list includes the EHT antennas that are already available and will be available in the nearest future: Kitt Peak and NOEMA (2021), former
385 CARMA antenna (2023).

All calculations were performed in Astro Space Locator software package for VLBI data reduction [45]. To reconstruct the synthesized beams we used uniform weighing with grid size of 1024×1024 corresponding to the field of view

$50 \times 50 \mu\text{as}$. As a kernel function we took an average function.

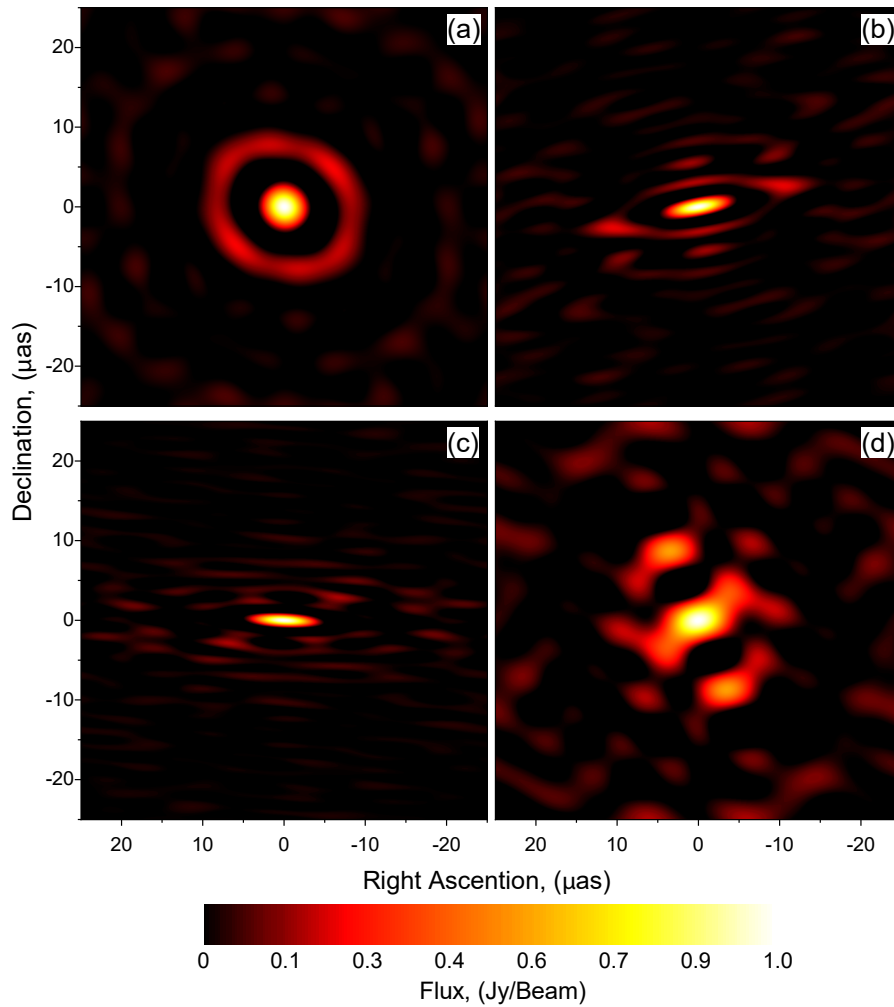


Figure 4: Synthesized beams for M87 target source: (a) – circular near-Earth orbit, (b) – HEO with 40000 km perigee, (c) – HEO with 100000 km perigee, (d) – L2 point orbit.

390 Image recovery procedure implies sequential subtracting of the beam from the maxima of the dirty map (for more details see [24], section 11.1 and [46]). Based on this principle, it can be concluded that beam configuration for the corresponding (u, v) -coverage defines the resulting quality of image recovery. For example, in case of large sidelobes in a beam false components could arise,

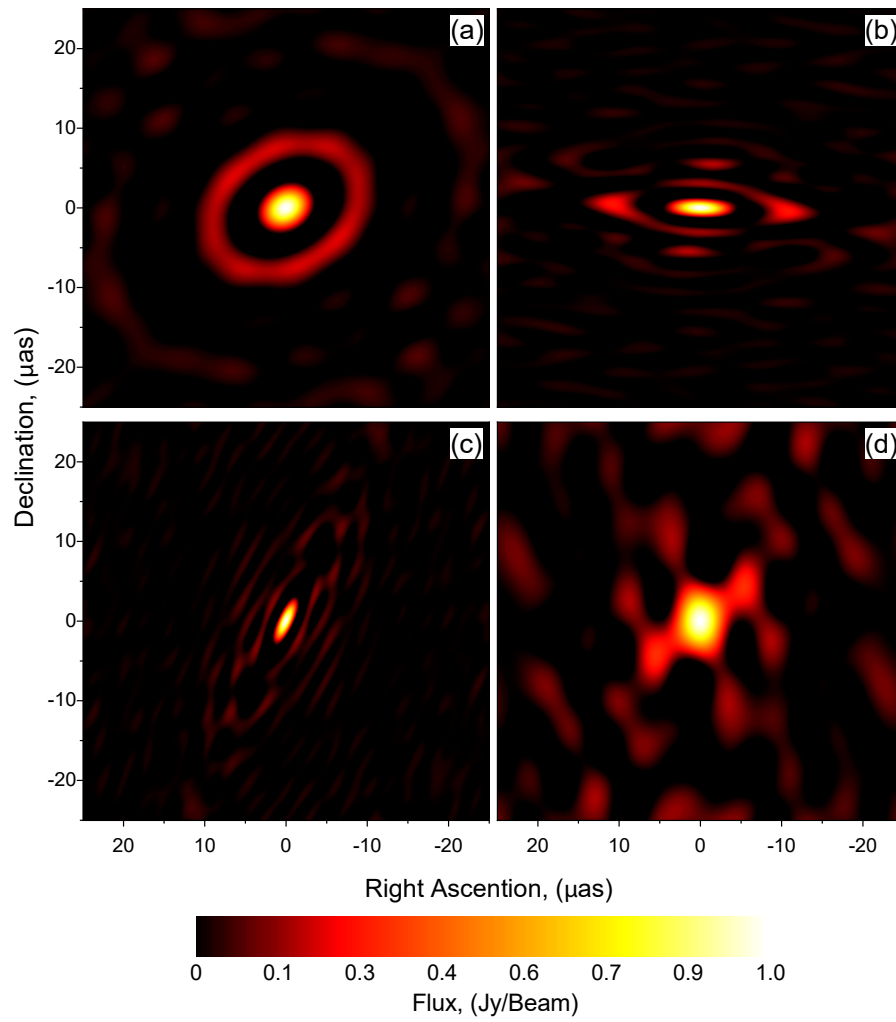


Figure 5: Synthesized beams for Sgr A* target source: (a) – circular near-Earth orbit, (b) – HEO with 40000 km perigee, (c) – HEO with 100000 km perigee, (d) – L2 point orbit.

Table 4: Beam parameters.

Orbit	Beam size, (μas)
Circular (40000 km) M87	4.4×4.0
Circular (40000 km) Sgr A*	5.0×3.8
HEO M87 (Perigee 40000 km)	6.0×1.6
HEO M87 (Perigee 100000 km)	6.2×1.2
HEO Sgr A* (Perigee 40000 km)	5.7×1.6
HEO Sgr A* (Perigee 100000 km)	4.3×1.2
L2 Orbit M87	6.5×4.3
L2 Orbit Sgr A*	6.9×4.9

395 creating artifacts in the resulting image. Asymmetrical elongated beam make it difficult to recover images. Based on this we can conclude that the best beam will be a symmetrical (circular) beam with dimensions at half maximum about $5 \mu\text{as}$ in the case of mapping sources such as SMBH, for example, Sgr A* or M87).

400 Fig. 4 and 5 show the obtained beams for different orbits for M87 and Sgr A* sources correspondingly. Obviously, the best radial symmetry is achieved with a circular orbit (Fig. 4, 5 (a)). In case of a high elliptical orbit (Fig. 4, 5 (b) and (c)), it is radially elongated in one of the directions. For an orbit around the L2 point (Fig. 4, 5 (d)), the beam has a number of interesting properties.
405 It has a radial symmetry comparing to HEO orbit, albeit not as much as for a circular one. At the same time, its dimensions allow to perform imaging with a resolution of about $5 \mu\text{as}$ (see Table 4). Achievable angular resolution of each orbit configuration presented in Table 5.

Maximum baseline projection for ground array of the EHT at 230 GHz
410 reached the values of about $25 \mu\text{as}$ [47], while space VLBI with the Radioastron yield the resolution of $8 \mu\text{as}$ at 1.3 cm [31]. The resolution from the estimated beams for considered orbital configurations demonstrates the increase in angular resolution for imaging comparing to the previous observations reaching $\approx 5 \mu\text{as}$

Table 5: The best and the worst angular resolution achievable for considered orbits.

Orbit	Angular Resolution (best - worst), μas				
	43 GHz	90 GHz	240 GHz	330 GHz	570 GHz
Circular	36 – 133	18 – 56	5.9 – 20	4.8 – 15	2.2 – 7.0
HEO	4.5 – 4500	2.1 – 2145	0.8 – 800	0.6 – 585	0.27 – 280
L2	0.8 – 550	0.4 – 265	0.14 – 100	0.1 – 72	0.05 – 35

at 230 GHz for all orbits. Speaking about the best achievable angular resolution
 415 L2 orbit will provide the highest angular resolution less than 1 μas . However
 this is true for the short survey observations and not for the full imaging.

4.3.1. Snapshot Mode

The snapshot (u, v) coverage is critical to imaging science. The point is that
 a detailed study of the dynamics of the close vicinity of black holes, the structure
 420 of which can be rapidly changing (for example, Sgr A* $\tau \sim 221$ s), requires a
 qualitative instantaneous (snapshot) (u, v) coverage which should accumulate
 in a short time comparable to the source variability. Fig. 7 shows the resulting
 snapshot (u, v) coverages for four orbital configurations: circular, two highly-
 elliptical orbits and L2 point orbit.

425 The calculated snapshots had a duration of ~ 4 minutes. However, we were
 unable to restore the synthesized beam as all of the (u, v) coverages are too
 sparse. Previously, in [12] a possibility to perform space-VLBI dynamical ob-
 servations of Sgr A* was demonstrated, but for different HEO configuration
 with a low perigee of ~ 10000 km. However, the thermal regime requirements
 430 do not allow implementation of an orbit with such a low perigee. Orbital con-
 figurations considered in this work are not capable of dynamic observations of
 such variable sources as Sgr A* and suggest only averaged observations.

4.3.2. Multi-band Observations

Space-ground VLBI differs from the ground-based observations with its rather
 435 sparse (u, v) coverage. However, one way to improve both the coverage and res-

olution is to use multi-frequency observation [48, 49]. Millimetron observatory will be capable to observe at several frequencies simultaneously. Therefore we have estimated the (u, v) coverage for 230+345 GHz observations with Millimetron and EHT ground telescopes for the case of L2 point orbit. Below
 440 Fig. 7 (a) and (b) show the (u, v) coverages for 230 GHz and 230+345 GHz observations and Fig. 7 (c) and (d) show the corresponding synthesized beams.

Adding up one more frequency slightly improves the situation with the side-lobes and the angular resolution: $6.5 \times 4.3 \mu\text{as}$ beams size for 230 GHz and $4.9 \times 3.0 \mu\text{as}$ 230+345 GHz correspondingly.

445 In addition to the improvement of (u, v) coverage and resolution, multi-frequency observations can help to increase the coherent integration time using phase transfer methods, which is valuable for the ground part of millimeter wavelength range VLBI observations [50, 51].

4.4. Source Visibility

450 Both for L2 and near-Earth orbits only 7 sources from the initial list are not visible: 0506-612, 0637-752, 1642+690, 1656+602, 1807+698, 1823+689, 1842+681, 1849+670, 1933+655. Thus, 379 out of 386 considered sources are available for space-ground observations with Millimetron.

455 Fig. 8 shows the annual visibility windows for Sgr A* and M87 sources for 4 years of mission operation. Blank regions correspond to the case when the sources are not available for observations due to the Sun constraints. Thus, VLBI observations at short baseline projections are possible once per year.

Fig. 9 shows the number of sources depending on the percentage of observable time during 4 years of mission operation. L2 orbit provide larger number of
 460 sources that are observable in 40% of 4 years of mission operation time, while for near-Earth orbits (HEO and circular) there are additional constraints of the Sun, the Moon and the Earth that reduce the total observing time to 20-30%.

Although the considered orbits were optimized primarily for observations of two target sources – Sgr A* and M87, there is also the possibility of observing

465 and imaging the sources that are close to the orbital plane of the spacecraft.
These could be for example: M84, 3C454 or OJ287.

5. Discussion and Conclusions

We have calculated several orbital configurations: circular near-Earth orbit with radius of 40000 km, two highly elliptical orbits with 40000 and 100000 km
470 perigee and L2 orbit with an exit from the ecliptic plane of 400000 km.

Due to the requirements for the thermal regime of the antenna and onboard scientific payload of the single-dish mode, the orbit around L2 point of Sun-Earth is considered as the main orbit of the Millimetron observatory. All other calculated orbits were considered as the possible second stage.

475 Each orbital configuration then was analyzed from a technical and scientific points of view. This analysis consisted of several steps: evaluation of synthesized beam, quantitative estimation of the number of observable sources, calculations for impulse and fuel costs for orbital corrections and transfer to/from Sun-Earth L2 point. From the point of view of VLBI imaging observations, namely
480 the quality of (u, v) coverage, the best orbital configuration is circular orbit. However, the results of fuel costs calculations demonstrate that it is impossible to organize a combined "L2 point+circular near-Earth orbit", while circular orbit itself doesn't meet the requirements for the single-dish observations due to the constraints of the Earth, the Sun and the Moon and their regular exposure
485 of the observatory.

High elliptical near-Earth orbits have a potential to perform the transfer to/from the L2 point of Sun-Earth system using the gravitational maneuvers. For our fuel estimations we considered a direct transfer to/from L2 point and in this case HEO orbits are still above the limits of the amount of available fuel.
490 Thermal regime of the observatory applies constraint on the perigee – it must be not lower than ~ 40000 km leading to drop in the (u, v) coverage quality for VLBI imaging and making such dynamic observations that are mentioned in [12] impossible. Here we did not provide an analysis of the possibility of transferring

between orbits using gravity assist maneuvers, since this is a separate study
495 performed out of the scope of this work.

From the point of view of the single-dish observations, the best possible
orbital configuration for Millimetron observatory will be orbit around L2 point
of Sun-Earth system. At the same time we have demonstrated that L2 point
orbit can provide shorter baselines (less than 5 Earth diameters) which means
500 that there is a possibility to perform VLBI imaging once per year for several
given target sources. Such limits arise from the constraints applied by the Sun.
Synthesized beam of L2 point orbit demonstrates a lower quality comparing
to the near-Earth orbits due to more sparse (u, v) coverage which however can
be improved by multi-band observations. Moreover, estimated source visibility
505 at L2 point orbit is 30% better comparing to the near-Earth orbits that have
additional constraints from the Sun, the Moon and the Earth.

Thus, the calculated orbit around L2 point is now suggested as a the new
nominal orbit. We believe that optimizing such L2 point orbit is more practical
approach than developing a two stage mission program with transfer between
510 the orbits.

Regarding the imaging capabilities of different orbital configurations, a more
detailed analysis can be found in [12?], where various models of sources are
considered and the sensitivity of the interferometer is analyzed.

It should also be borne in mind that the calculated orbits belong to their
515 families of orbits and may be changed and optimized depending on the final
spacecraft launch date and the final scientific program and requirements.

References

- [1] N. S. Kardashev, I. D. Novikov, V. N. Lukash, S. V. Pilipenko, E. V.
Mikheeva, D. V. Bisikalo, D. S. Wiebe, A. G. Doroshkevich, A. V. Zasov,
520 I. I. Zinchenko, P. B. Ivanov, V. I. Kostenko, T. I. Larchenkova, S. F.
Likhachev, I. F. Malov, V. M. Malofeev, A. S. Pozanenko, A. V. Smirnov,
A. M. Sobolev, A. M. Cherepashchuk, Y. A. Shchekinov, Review of sci-

entific topics for the Millimetron space observatory, *Physics Uspekhi* 57 (2014) 1199–1228. [arXiv:1502.06071](https://arxiv.org/abs/1502.06071), [doi:http://doi.org/10.3367/UFNe.0184.201412c.1319](http://doi.org/10.3367/UFNe.0184.201412c.1319).

525

[2] H. Hirosawa, H. Hirabayashi, H. Kobayashi, Y. Murata, T. Kii, P. Edwards, M. Natori, T. Takano, Z.-I. Yamamoto, T. Hashimoto, K. Inoue, A. Ohnishi, T. Ohshima, T. Ichikawa, K. Fujisawa, K. Wajima, R. Okayasu, M. Inoue, N. Kawaguchi, S. Kameno, K. Shibata, Y. Asaki, Space vlbi satellite halca and its engineering accomplishments, *Acta Astronautica* 50 (5) (2002) 301–309. [doi:https://doi.org/10.1016/S0094-5765\(01\)00171-0](https://doi.org/10.1016/S0094-5765(01)00171-0).
URL <https://www.sciencedirect.com/science/article/pii/S0094576501001710>

530

[3] N. S. Kardashev, V. V. Khartov, V. V. Abramov, V. Y. Avdeev, A. V. Alakoz, Y. A. Aleksandrov, S. Ananthakrishnan, V. V. Andreyanov, A. S. Andrianov, N. M. Antonov, M. I. Artyukhov, M. Y. Arkhipov, W. Baan, N. G. Babakin, V. E. Babyshkin, N. Bartel', K. G. Belousov, A. A. Belyaev, J. J. Berulis, B. F. Burke, A. V. Biryukov, A. E. Bubnov, M. S. Burgin, G. Busca, A. A. Bykadorov, V. S. Bychkova, V. I. Vasil'kov, K. J. Wellington, I. S. Vinogradov, R. Wietfeldt, P. A. Voitsik, A. S. Gvamichava, I. A. Girin, L. I. Gurvits, R. D. Dagkesamanskii, L. D'Addario, G. Giovannini, D. L. Jauncey, P. E. Dewdney, A. A. D'yakov, V. E. Zharov, V. I. Zhuravlev, G. S. Zaslavskii, M. V. Zakhvatkin, A. N. Zinov'ev, Y. Ilinen, A. V. Ipatov, B. Z. Kanevskii, I. A. Knorin, J. L. Casse, K. I. Kellermann, Y. A. Kovalev, Y. Y. Kovalev, A. V. Kovalenko, B. L. Kogan, R. V. Komaev, A. A. Konovalenko, G. D. Kopelyanskii, Y. A. Korneev, V. I. Kostenko, A. N. Kotik, B. B. Kreisman, A. Y. Kukushkin, V. F. Kulishenko, D. N. Cooper, A. M. Kut'kin, W. H. Cannon, M. G. Lari-onov, M. M. Lisakov, L. N. Litvinenko, S. F. Likhachev, L. N. Likhacheva, A. P. Lobanov, S. V. Logvinenko, G. Langston, K. McCracken, S. Y. Medvedev, M. V. Melekhin, A. V. Menderov, D. W. Murphy, T. A.

545

550

- Mizyakina, Y. V. Mozgvoi, N. Y. Nikolaev, B. S. Novikov, I. D. Novikov,
V. V. Oreshko, Y. K. Pavlenko, I. N. Pashchenko, Y. N. Ponomarev,
555 M. V. Popov, A. Pravin-Kumar, R. A. Preston, V. N. Pyshnov, I. A.
Rakhimov, V. M. Rozhkov, J. D. Romney, P. Rocha, V. A. Rudakov,
A. Räsänen, S. V. Sazankov, B. A. Sakharov, S. K. Semenov, V. A. Sere-
brennikov, R. T. Schilizzi, D. P. Skulachev, V. I. Slysh, A. I. Smirnov,
J. G. Smith, V. A. Soglasnov, K. V. Sokolovskii, L. H. Sondaar, V. A.
560 Stepan'yants, M. S. Turygin, S. Y. Turygin, A. G. Tuchin, S. Urpo, S. D. Fe-
dorchuk, A. M. Finkel'shtein, E. B. Fomalont, I. Fejes, A. N. Fomina, Y. B.
Khapin, G. S. Tsarevskii, J. A. Zensus, A. A. Chuprikov, M. V. Shatskaya,
N. Y. Shapirovskaya, A. I. Sheikhet, A. E. Shirshakov, A. Schmidt, L. A.
Shnyreva, V. V. Shpilevskii, R. D. Ekers, V. E. Yakimov, "RadioAstron"-A
565 telescope with a size of 300 000 km: Main parameters and first observa-
tional results, *Astronomy Reports* 57 (2013) 153–194. [arXiv:1303.5013](https://arxiv.org/abs/1303.5013),
[doi:http://doi.org/10.1134/S1063772913030025](https://doi.org/10.1134/S1063772913030025).
- [4] C. R. Gwinn, Y. Y. Kovalev, M. D. Johnson, V. A. Soglasnov, Discovery of
Substructure in the Scatter-broadened Image of Sgr A*, *The Astrophysical*
570 *Journal Letters* 794 (1) (2014) L14. [arXiv:1409.0530](https://arxiv.org/abs/1409.0530), [doi:http://doi.](https://doi.org/10.1088/2041-8205/794/1/L14)
[org/10.1088/2041-8205/794/1/L14](https://doi.org/10.1088/2041-8205/794/1/L14).
- [5] M. D. Johnson, R. Narayan, The Optics of Refractive Substructure, *The*
Astrophysical Journal 826 (2) (2016) 170. [arXiv:1606.06315](https://arxiv.org/abs/1606.06315), [doi:http://http:](https://doi.org/10.3847/0004-637X/826/2/170)
[//doi.org/10.3847/0004-637X/826/2/170](https://doi.org/10.3847/0004-637X/826/2/170).
- 575 [6] M. D. Johnson, R. Narayan, D. Psaltis, L. Blackburn, Y. Y. Kovalev, C. R.
Gwinn, G.-Y. Zhao, G. C. Bower, J. M. Moran, M. Kino, M. Kramer,
K. Akiyama, J. Dexter, A. E. Broderick, L. Sironi, The Scattering and
Intrinsic Structure of Sagittarius A* at Radio Wavelengths, *The Astro-*
physical Journal 865 (2018) 104. [arXiv:1808.08966](https://arxiv.org/abs/1808.08966), [doi:http://doi.](https://doi.org/10.3847/1538-4357/aadcff)
580 [org/10.3847/1538-4357/aadcff](https://doi.org/10.3847/1538-4357/aadcff).
- [7] V. L. Fish, M. Shea, K. Akiyama, Imaging black holes and jets with a

VLBI array including multiple space-based telescopes, *Advances in Space Research* 65 (2) (2020) 821–830. [arXiv:1903.09539](https://arxiv.org/abs/1903.09539), [doi:10.1016/j.asr.2019.03.029](https://doi.org/10.1016/j.asr.2019.03.029).

585 [8] D. C. M. Palumbo, S. S. Doeleman, M. D. Johnson, K. L. Bouman, A. A. Chael, Metrics and Motivations for Earth-Space VLBI: Time-resolving Sgr A* with the Event Horizon Telescope, *The Astrophysical Journal* 881 (1) (2019) 62. [arXiv:1906.08828](https://arxiv.org/abs/1906.08828), [doi:10.3847/1538-4357/ab2bed](https://doi.org/10.3847/1538-4357/ab2bed).

[9] A. W. Raymond, D. Palumbo, S. N. Paine, L. Blackburn, R. Córdoba
590 Rosado, S. S. Doeleman, J. R. Farah, M. D. Johnson, F. Roelofs, R. P. J. Tilanus, J. Weintroub, Evaluation of New Submillimeter VLBI Sites for the Event Horizon Telescope, *The Astrophysical Journal Supplement Series* 253 (1) (2021) 5. [arXiv:2102.05482](https://arxiv.org/abs/2102.05482), [doi:10.3847/1538-3881/abc3c3](https://doi.org/10.3847/1538-3881/abc3c3).

[10] X. Hong, Z. Shen, T. An, Q. Liu, The chinese space millimeter-
595 wavelength vlbi array—a step toward imaging the most compact astronomical objects, *Acta Astronautica* 102 (2014) 217–225. [doi:https://doi.org/10.1016/j.actaastro.2014.05.026](https://doi.org/10.1016/j.actaastro.2014.05.026).
URL <https://www.sciencedirect.com/science/article/pii/S0094576514001970>

600 [11] F. Roelofs, H. Falcke, C. Brinkerink, M. Mościbrodzka, L. I. Gurvits, M. Martin-Neira, V. Kudriashov, M. Klein-Wolt, R. Tilanus, M. Kramer, L. Rezzolla, Simulations of imaging the event horizon of Sagittarius A* from space, *Astronomy and Astrophysics* 625 (2019) A124. [arXiv:1904.04934](https://arxiv.org/abs/1904.04934), [doi:http://doi.org/10.1051/0004-6361/201732423](https://doi.org/10.1051/0004-6361/201732423).

605 [12] A. S. Andrianov, A. M. Baryshev, H. Falcke, I. A. Girin, T. de Graauw, V. I. Kostenko, V. Kudriashov, V. A. Ladygin, S. F. Likhachev, F. Roelofs, A. G. Rudnitskiy, A. R. Shaykhutdinov, Y. A. Shchekinov, M. A. Shchurov, Simulations of M87 and Sgr A* imaging with the Millimetron Space Observatory on near-Earth orbits, *Monthly Notices of the Royal Astronomical Society* 500 (4) (2020) 4866–4877. [arXiv:https://academic.oup.com/](https://arxiv.org/abs/https://academic.oup.com/)
610

`mnras/article-pdf/500/4/4866/34861444/staa2709.pdf`, doi:<http://doi.org/10.1093/mnras/staa2709>.
URL <https://doi.org/10.1093/mnras/staa2709>

- [13] C. Petretti, V. Fish, K. Akiyama, Simulating Observations of M87 with
615 the Event Horizon Telescope and Space VLBI, in: American Astronomical Society Meeting Abstracts, Vol. 53 of American Astronomical Society Meeting Abstracts, 2021, p. 152.01.
- [14] Event Horizon Telescope Collaboration, K. Akiyama, A. Alberdi, W. Alef,
K. Asada, R. Azulay, A.-K. Baczko, D. Ball, M. Baloković, J. Barrett, et al.,
620 First M87 Event Horizon Telescope Results. VI. The Shadow and Mass of the Central Black Hole, *The Astrophysical Journal Letters* 875 (2019) L6. [arXiv:1906.11243](https://arxiv.org/abs/1906.11243), doi:<http://doi.org/10.3847/2041-8213/ab1141>.
- [15] M. Martin-Neira, V. Kudriashov, I. Barat, B. Duesmann, E. Daganzo,
625 Space-to-space radio interferometry system from medium earth orbits, *Chinese Journal of Space Science* 39 (4) (2019) 544. doi:<http://doi.org/10.11728/cjss2019.04.544>.
URL http://www.cjss.ac.cn/EN/abstract/article_2750.shtml
- [16] V. Kudriashov, M. Martin-Neira, I. Barat, P. Martin Iglesias, E. Daganzo-
Eusebio, N. Alagha, V. Valenta, System design for the event horizon imag-
630 ing experiment using the pecmeo concept, *Chinese Journal of Space Science* 39 (2) (2019) 250. doi:<http://doi.org/10.11728/cjss2019.02.250>.
URL http://www.cjss.ac.cn/EN/abstract/article_2693.shtml
- [17] M. D. Johnson, C. R. Gwinn, Theory and Simulations of Refractive Sub-
structure in Resolved Scatter-broadened Images, *The Astrophysical Journal*
635 805 (2) (2015) 180. [arXiv:1502.05722](https://arxiv.org/abs/1502.05722), doi:<http://doi.org/10.1088/0004-637X/805/2/180>.
- [18] S. T. Han, J. W. Lee, J. Kang, C. S. Oh, D. Y. Byun, D. H. Je, M. H. Chung,
S. Y. Kim, S. O. Wi, M. Song, Y. W. Kang, Korean VLBI Network receiver

- optics for simultaneous multi-frequency observation, in: Proceedings of the
640 11th European VLBI Network Symposium & Users Meeting. 9-12 October,
2012, p. 59.
- [19] S.-T. Han, J.-W. Lee, B. Lee, M.-H. Chung, S.-M. Lee, D.-H. Je, S.-O. Wi,
P. F. Goldsmith, A Millimeter-Wave Quasi-Optical Circuit for Compact
Triple-Band Receiving System, *Journal of Infrared* 38 (12) (2017) 1487–
645 1501. doi:10.1007/s10762-017-0438-2.
- [20] N. A. Demidov, A. A. Belyaev, V. A. Polyakov, Y. V. Timofeev, On-
board Hydrogen Frequency Standard for the Millimetron Space Ob-
servatory, *Measurement Techniques* 61 (2018) 791–796. doi:10.1007/
s11018-018-1503-5.
- 650 [21] T. D. Papanikolaou, D. Tsoulis, Assessment of numerical integration meth-
ods in the context of low Earth orbits and inter-satellite observation
analysis, *Acta Geodaetica et Geophysica* 51 (2016) 619–641. doi:http:
//doi.org/10.1007/s40328-016-0159-3.
- [22] J. Schall, T. Mayer-Gürr, A. Eicker, J. Kusche, A Global Gravitational
655 Field Model from GOCE Gradiometer Observations, in: L. Ouwehand
(Ed.), 4th International GOCE User Workshop, Vol. 696 of ESA Special
Publication, 2011, p. 12.
- [23] J. Butcher, *Numerical Methods for Ordinary Differential Equations*, Second
Edition, John Wiley & Sons, Ltd, 2008. doi:http://doi.org/10.1002/
660 9780470753767.
- [24] A. R. Thompson, J. M. Moran, J. Swenson, George W., *Interferometry
and Synthesis in Radio Astronomy*, 3rd Edition, Springer, Cham, 2017.
doi:http://doi.org/10.1007/978-3-319-44431-4.
- [25] L. Liu, W. Zheng, The optimization of satellite orbit for Space-VLBI ob-
665 servation, *Research in Astronomy and Astrophysics* 21 (2) (2021) 037.

- [26] L. Combrinck, *Satellite Laser Ranging*, 2010, pp. 301–338. doi:10.1007/978-3-642-11741-1_9, .
- [27] X. Sun, P. Chen, C. Macabiau, C. Han, Low-earth orbit determination from gravity gradient measurements, *Acta Astronautica* 123 (2016) 350–362, special Section: Selected Papers from the International Workshop on Satellite Constellations and Formation Flying 2015. doi:<https://doi.org/10.1016/j.actaastro.2016.03.012>.
URL <https://www.sciencedirect.com/science/article/pii/S0094576515301193>
- [28] T. Basar, *A new approach to linear filtering and prediction problems* (2009) 167–179doi:10.1109/9780470544334.ch9.
- [29] R. Nazirov, N. Eismont, V. Arefiev, F. Korotkov, A. Pogodin, A. Tregubov, A. Ditrikh, *Mission Design Problems for the Spectrum-Roentgen-Gamma Project*, *Cosmic Research* 57(1) (2019) 61–67.
- [30] N. S. Kardashev, A. V. Alakoz, Y. Y. Kovalev, M. V. Popov, A. M. Sobolev, K. V. Sokolovsky, *Radioastron: Main results of the implementation of the early science program in studies of astronomical objects in the universe with ultra-high angular resolution*, *Solar System Research* 49 (2015) 573–579. doi:<http://doi.org/10.1134/S0038094615070096>.
- [31] Y. Y. Kovalev, N. S. Kardashev, K. V. Sokolovsky, P. A. Voitsik, T. An, J. M. Anderson, A. S. Andrianov, V. Y. Avdeev, N. Bartel, H. E. Bignall, M. S. Burgin, P. G. Edwards, S. P. Ellingsen, S. Frey, C. García-Miró, M. P. Gawroński, F. D. Ghigo, T. Ghosh, G. Giovannini, I. A. Girin, M. Giroletti, L. I. Gurvits, D. L. Jauncey, S. Horiuchi, D. V. Ivanov, M. A. Kharinov, J. Y. Koay, V. I. Kostenko, A. V. Kovalenko, Y. A. Kovalev, E. V. Kravchenko, M. Kunert-Bajraszewska, A. M. Kutkin, S. F. Likhachev, M. M. Lisakov, I. D. Litovchenko, J. N. McCallum, A. Melis, A. E. Melnikov, C. Migoni, D. G. Nair, I. N. Pashchenko, C. J. Phillips, A. Polatidis, A. B. Pushkarev, J. F. H. Quick, I. A. Rakhimov, C. Reynolds, J. R. Rizzo,

- 695 A. G. Rudnitskiy, T. Savolainen, N. N. Shakhvorostova, M. V. Shatskaya,
Z. Q. Shen, M. A. Shchurov, R. C. Vermeulen, P. de Vicente, P. Wolak, J. A.
Zensus, V. A. Zuga, Detection statistics of the RadioAstron AGN survey,
Advances in Space Research 65 (2) (2020) 705–711. [arXiv:1909.00785](https://arxiv.org/abs/1909.00785),
[doi:http://doi.org/10.1016/j.asr.2019.08.035](https://doi.org/10.1016/j.asr.2019.08.035).
- 700 [32] H. Hirabayashi, H. Hirosawa, The VSOP Mission: A General Introduction
and Current Overview, Advances in Space Research 26 (4) (2000) 589–595.
[doi:http://doi.org/10.1016/S0273-1177\(99\)01174-6](https://doi.org/10.1016/S0273-1177(99)01174-6).
- [33] M. Tsuboi, VSOP-2/ASTRO-G Project Team, VSOP-2/ASTRO-G Project
Overview for the Astronomy Community, in: Y. Hagiwara, E. Fomalont,
705 M. Tsuboi, M. Yasuhiro (Eds.), Approaching Micro-Arcsecond Resolution
with VSOP-2: Astrophysics and Technologies, Vol. 402 of Astronomical
Society of the Pacific Conference Series, 2009, p. 30.
- [34] N. S. Kardashev, B. B. Kreisman, A. V. Pogodin, Y. N. Ponomarev, E. N.
Filippova, A. I. Sheikhet, Orbit design for the Spektr-R spacecraft of the
710 ground-space interferometer, Cosmic Research 52 (5) (2014) 332–341. [doi :](https://doi.org/10.1134/S0010952514050050)
[http://doi.org/10.1134/S0010952514050050](https://doi.org/10.1134/S0010952514050050).
- [35] M. V. Zakhvatkin, Y. N. Ponomarev, V. A. Stepan'yants, A. G. Tuchin,
G. S. Zaslavskiy, Navigation support for the RadioAstron mission, Cos-
mic Research 52 (5) (2014) 342–352. [doi:http://doi.org/10.1134/](https://doi.org/10.1134/S0010952514050128)
715 [S0010952514050128](https://doi.org/10.1134/S0010952514050128).
- [36] M. Pavlinsky, V. Levin, V. Akimov, A. Krivchenko, A. Rotin,
M. Kuznetsova, I. Lapshov, A. Tkachenko, R. Krivonos, N. Semena,
M. Buntov, A. Glushenko, V. Arefiev, A. Yaskovich, S. Grebenev,
S. Sazonov, A. Lutovinov, S. Molkov, D. Serbinov, M. Kudelin, T. Droz-
720 dova, S. Voronkov, R. Sunyaev, E. Churazov, M. Gilfanov, B. Ramsey, S. L.
O'Dell, J. Kolodziejczak, V. Zavlin, D. Swartz, ART-XC / SRG overview,
in: J.-W. A. den Herder, S. Nikzad, K. Nakazawa (Eds.), Space Telescopes

- and Instrumentation 2018: Ultraviolet to Gamma Ray, Vol. 10699, International Society for Optics and Photonics, SPIE, 2018, pp. 468 – 477.
725 doi:10.1117/12.2312053.
URL <https://doi.org/10.1117/12.2312053>
- [37] S. D. Glazer, K. D. Brown, T. J. Michalek, W. C. Ancarrow, WMAP Observatory Thermal Design and On-Orbit Thermal Performance, *Journal of Aerospace* 112 (2003) 92–102.
- 730 [38] J. P. Gardner, J. C. Mather, M. Clampin, R. Doyon, M. A. Greenhouse, H. B. Hammel, J. B. Hutchings, P. Jakobsen, S. J. Lilly, K. S. Long, J. I. Lunine, M. J. McCaughrean, M. Mountain, J. Nella, G. H. Rieke, M. J. Rieke, H.-W. Rix, E. P. Smith, G. Sonneborn, M. Stiavelli, H. S. Stockman, R. A. Windhorst, G. S. Wright, The James Webb Space Telescope, *Space*
735 *Science Reviews* 123 (4) (2006) 485–606. arXiv:astro-ph/0606175, doi:
<http://doi.org/10.1007/s11214-006-8315-7>.
- [39] T. Passvogel, G. Crone, O. Piersanti, B. Guillaume, J. Tauber, J. M. Reix, T. Banos, P. Rideau, B. Collaudin, Planck an Overview of the
740 *Spacecraft*, in: J. G. Weisend (Ed.), *Transactions of the Cryogenic Engineering Conference - CEC: Advances in Cryogenic Engineering*, Vol. 1218 of American Institute of Physics Conference Series, 2010, pp. 1494–1501.
doi:<http://doi.org/10.1063/1.3422328>.
- [40] M. Sánchez-Portal, G. L. Pilbratt, The Herschel Space Observatory: Mission Overview and Observing Opportunities, *Astrophysics and Space*
745 *Science Proceedings* 14 (2010) 537. doi:http://doi.org/10.1007/978-3-642-11250-8_165.
- [41] Gaia Collaboration, The Gaia mission, *Astronomy and Astrophysics* 595 (2016) A1. arXiv:1609.04153, doi:<http://doi.org/10.1051/0004-6361/201629272>.
- 750 [42] A. Farres, C. Webster, D. Folta, High fidelity modeling of SRP and its

effect on the relative motion of Starshade and WFIRST, AIAA 2018 2018 (2018) 2227. doi:http://doi.org/10.1007/978-3-642-11250-8_165.

[43] I. D. Kovalenko, N. A. Eismont, Orbit design for the spectrum-roentgen-gamma mission, *Acta Astronautica* 160 (2019) 56 – 61. doi:<https://doi.org/10.1016/j.actaastro.2019.04.006>.

755 URL <http://www.sciencedirect.com/science/article/pii/S0094576518319295>

[44] Event Horizon Telescope Collaboration, First M87 Event Horizon Telescope Results. II. Array and Instrumentation, *The Astrophysical Journal Letters* 760 875 (1) (2019) L2. arXiv:1906.11239, doi:<http://doi.org/10.3847/2041-8213/ab0c96>.

[45] S. Likhachev, I. Girin, V. Y. Avdeev, A. Andrianov, M. Andrianov, V. Kostenko, V. Ladygin, A. Lyakhovets, I. Litovchenko, A. Rudnitskiy, M. Shchurov, N. Utkin, V. Zuga, Astro space locator – a software package for vlbi data processing and reduction, *Astronomy and Computing* 33 (2020) 100426. doi:<https://doi.org/10.1016/j.ascom.2020.100426>.

765 URL <http://www.sciencedirect.com/science/article/pii/S2213133720300809>

[46] J. A. Högbom, Aperture Synthesis with a Non-Regular Distribution of Interferometer Baselines, *Astronomy and Astrophysics Supplement Series* 15 (1974) 417.

[47] Event Horizon Telescope Collaboration, First M87 Event Horizon Telescope Results. I. The Shadow of the Supermassive Black Hole, *Astrophysical Journal Letters* 875 (1) (2019) L1. arXiv:1906.11238, doi:<http://doi.org/10.3847/2041-8213/ab0ec7>.

775 [48] S. Doleman, L. Blackburn, J. Dexter, J. L. Gomez, M. D. Johnson, D. C. Palumbo, J. Weintroub, J. R. Farah, V. Fish, L. Loinard, C. Lonsdale, G. Narayanan, N. A. Patel, D. W. Pesce, A. Raymond, R. Tilanus, M. Wielgus, K. Akiyama, G. Bower, A. Broderick, R. Deane, C. M. Fromm,

- 780 C. Gammie, R. Gold, M. Janssen, T. Kawashima, T. Krichbaum, D. P.
Marrone, L. D. Matthews, Y. Mizuno, L. Rezzolla, F. Roelofs, E. Ros,
T. K. Savolainen, F. Yuan, G. Zhao, L. Blackburn, S. Doeleman, J. Dex-
ter, J. L. Gomez, M. D. Johnson, D. C. Palumbo, J. Weintroub, J. R. Farah,
V. Fish, L. Loinard, C. Lonsdale, G. Narayanan, N. A. Patel, D. W. Pesce,
785 A. Raymond, R. Tilanus, M. Wielgus, K. Akiyama, G. Bower, A. Broderick,
R. Deane, C. M. Fromm, C. Gammie, R. Gold, M. Janssen, T. Kawashima,
T. Krichbaum, D. P. Marrone, L. D. Matthews, Y. Mizuno, L. Rezzolla,
F. Roelofs, E. Ros, T. K. Savolainen, F. Yuan, G. Zhao, Studying Black
Holes on Horizon Scales with VLBI Ground Arrays, in: Bulletin of the
790 American Astronomical Society, Vol. 51, 2019, p. 256. [arXiv:1909.01411](https://arxiv.org/abs/1909.01411).
- [49] M. Johnson, K. Haworth, D. W. Pesce, D. C. M. Palumbo, L. Black-
burn, K. Akiyama, D. Boroson, K. L. Bouman, J. R. Farah, V. L. Fish,
M. Honma, T. Kawashima, M. Kino, A. Raymond, M. Silver, J. Weintroub,
M. Wielgus, S. S. Doeleman, J. Kauffmann, G. K. Keating, T. P. Krich-
baum, L. Loinard, G. Narayanan, A. Doi, D. J. James, D. P. Marrone,
795 Y. Mizuno, H. Nagai, Studying black holes on horizon scales with space-
VLBI, in: Bulletin of the American Astronomical Society, Vol. 51, 2019, p.
235. [arXiv:1909.01405](https://arxiv.org/abs/1909.01405).
- [50] M. Rioja, R. Dodson, J. Gómez, S. Molina, T. Jung, B. Sohn, The Power
800 of (Near) Simultaneous Multi-Frequency Observations for mm-VLBI and
Astrometry, *Galaxies* 5 (1) (2017) 9. [doi:10.3390/galaxies5010009](https://doi.org/10.3390/galaxies5010009).
- [51] G.-Y. Zhao, J. C. Algaba, S. S. Lee, T. Jung, R. Dodson, M. Rioja, D.-
Y. Byun, J. Hodgson, S. Kang, D.-W. Kim, J.-Y. Kim, J.-S. Kim, S.-
W. Kim, M. Kino, A. Miyazaki, J.-H. Park, S. Trippe, K. Wajima, The
805 Power of Simultaneous Multi-frequency Observations for mm-VLBI: Be-
yond Frequency Phase Transfer, *The Astronomical Journal* 155 (1) (2018)
26. [arXiv:1712.06243](https://arxiv.org/abs/1712.06243), [doi:10.3847/1538-3881/aa99e0](https://doi.org/10.3847/1538-3881/aa99e0).

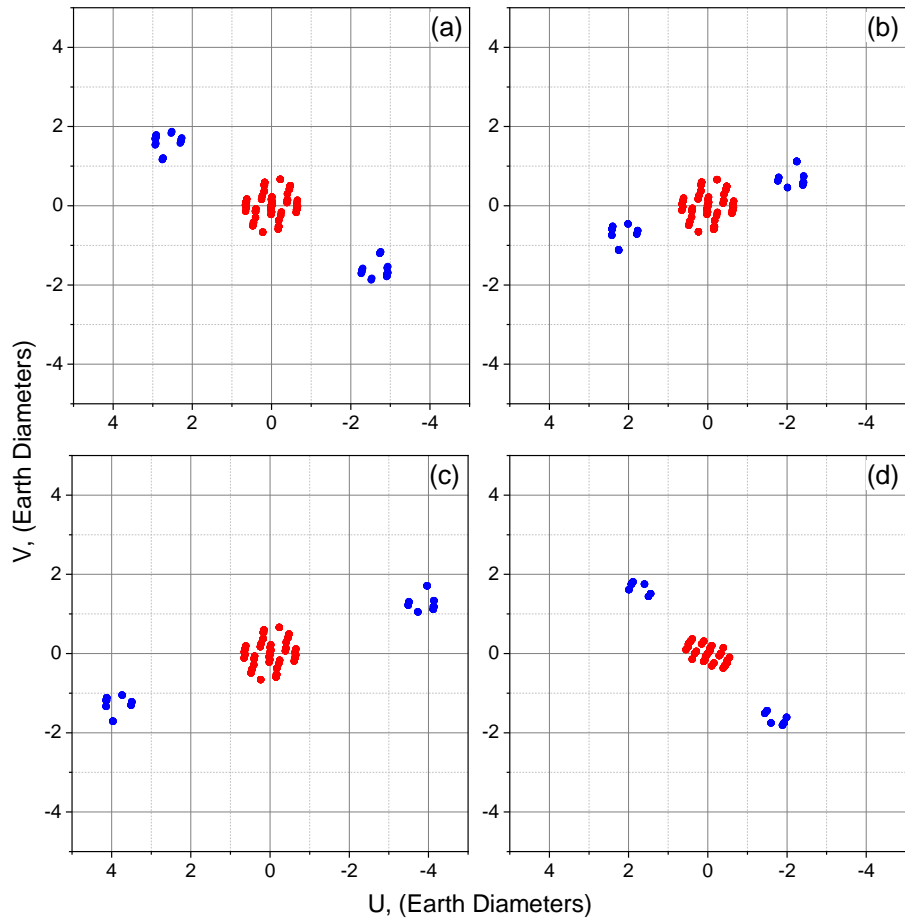


Figure 6: Snapshot (u, v) coverage for (a) – circular near-Earth orbit, (b) – high elliptical near-Earth orbit with 40000 km perigee, (c) – high elliptical near-Earth orbit with 100000 km perigee, (d) – orbit around L2 point of the Sun-Earth system.

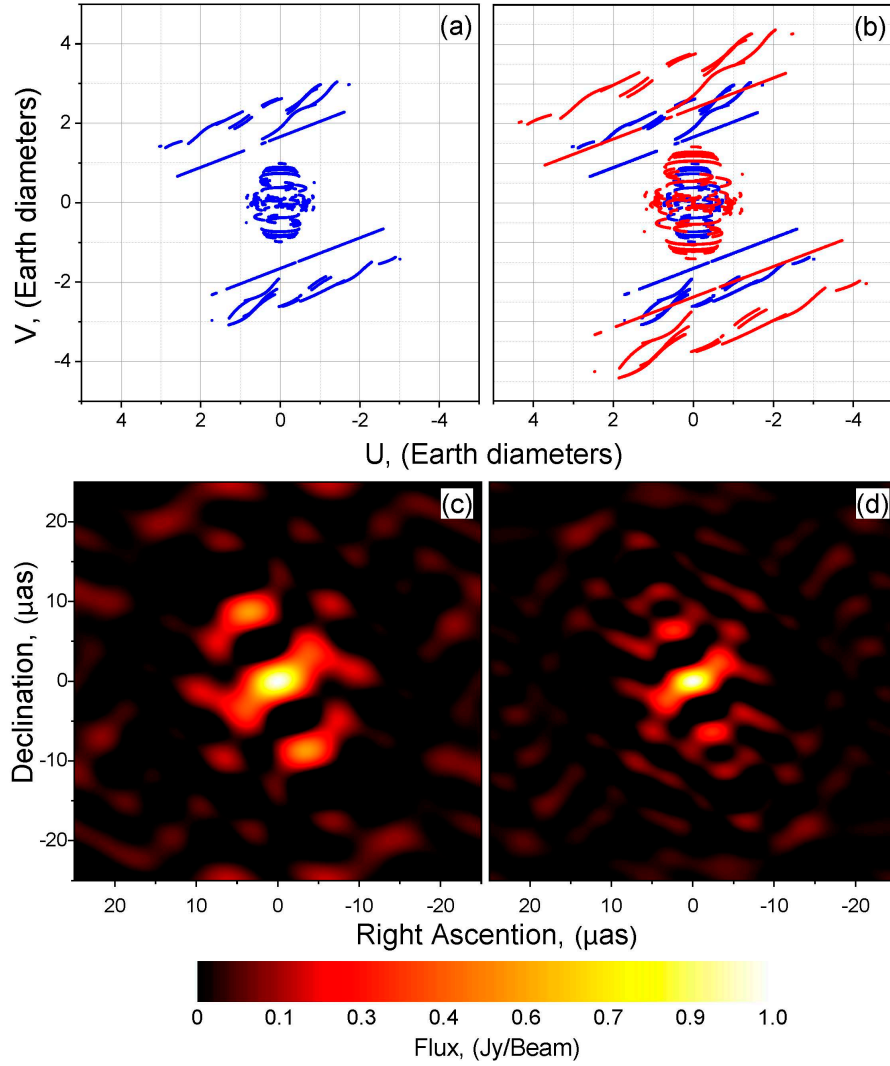


Figure 7: (u, v) coverage and synthesized beam for 230 GHz (a and c) and for multi-band 230+345 GHz (b and d) observations. Blue dots correspond to 230 GHz observations, red dots correspond to 230+345 GHz observations.

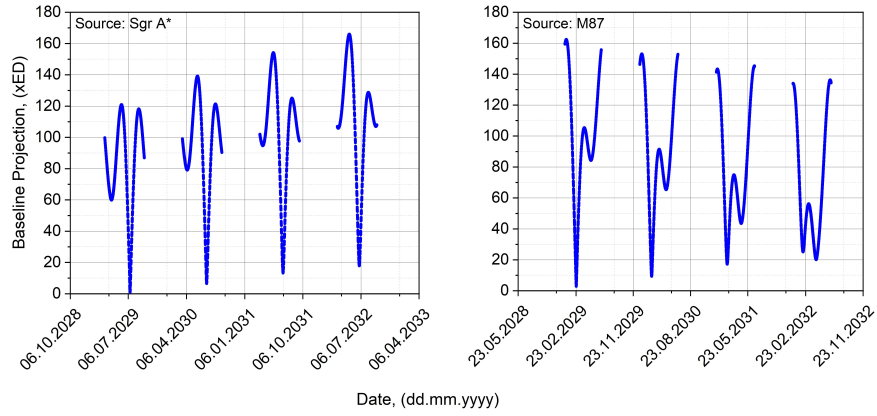


Figure 8: Baseline projection in time for Sgr A* (left) and M87 (right) for L2 point orbit. Time span – 4 years. Gaps correspond to the case when the sources are not observable due to the Sun constraints.

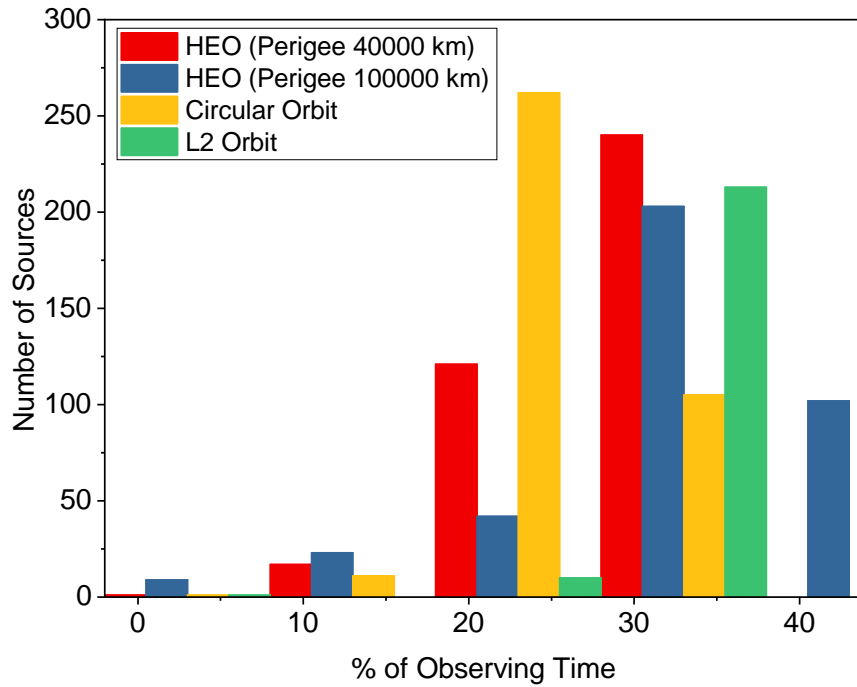


Figure 9: Number of sources vs. percentage of available observing time for them for 4 years of mission operation.